

Camera Intrinsic Calibration: Automated and Manual Methodologies

ECE 738 - Computer Vision, Spring 2026

Pavel Stepanov

Department of Electrical and Computer Engineering

University of Miami

Coral Gables, Florida, USA

pas273@miami.edu

Abstract—This paper presents a comprehensive camera intrinsic calibration study comparing automated and manual parameter estimation methodologies. Automated calibration using the Zhang method with a 14×10 checkerboard pattern across 21 images achieved a mean reprojection error of 2.27 pixels (0.075% of 3024×3024 resolution), well below the recommended threshold. Three manual experiments independently estimated aspect ratio, focal lengths, and principal point using geometric measurements and projection equations. Comparisons showed excellent agreement for aspect ratio (1.73% difference) and focal lengths (approximately 2% difference), with acceptable agreement for principal point (4–10% difference). The distortion model revealed moderate radial distortion coefficients ($k_1 = 0.061$, $k_2 = 0.687$, $k_3 = -2.84$) and minimal tangential distortion. The results validate both methodologies and demonstrate high-quality calibration suitable for precision computer vision applications including 3D reconstruction, augmented reality, and photogrammetry.

1. INTRODUCTION

Camera calibration is a fundamental procedure in computer vision that determines the intrinsic parameters of a camera and corrects for lens distortion. These parameters are essential for applications including 3D reconstruction, augmented reality, robot navigation, and photogrammetry. This work presents a comprehensive camera calibration study employing both automated and manual methodologies to validate parameter estimation accuracy.

The primary objectives of this investigation are to: (1) perform automated calibration using the Zhang method with checkerboard pattern detection, (2) independently estimate intrinsic parameters through manual experimental procedures, and (3) compare the two approaches to validate calibration accuracy. The camera intrinsic matrix contains focal lengths f_x and f_y , principal point coordinates (c_x, c_y) , and skew coefficient s , while the distortion model captures radial and tangential lens aberrations.

This paper is organized as follows: Section 2 provides theoretical background on camera geometry and calibration models. Section 3 details the experimental procedures for both automated and manual calibration. Section 4 presents quantitative results and comparative analysis. Section 5 discusses findings and sources of error. Section 6 concludes the work.

2. TECHNICAL BACKGROUND

A. Pinhole Camera Model

The pinhole camera model describes the geometric projection of 3D world points onto a 2D image plane. For a point $\mathbf{X} = [X, Y, Z]^T$ in world coordinates, its projection to image point $\mathbf{x} = [u, v]^T$ is given by:

$$s \begin{bmatrix} u \\ v \\ 1 \end{bmatrix} = \mathbf{K}[\mathbf{R}|\mathbf{t}] \begin{bmatrix} X \\ Y \\ Z \\ 1 \end{bmatrix} \quad (1)$$

where s is a scale factor, \mathbf{K} is the camera intrinsic matrix, \mathbf{R} is the rotation matrix, and \mathbf{t} is the translation vector. The intrinsic matrix \mathbf{K} encodes the internal camera parameters:

$$\mathbf{K} = \begin{bmatrix} f_x & s & c_x \\ 0 & f_y & c_y \\ 0 & 0 & 1 \end{bmatrix} \quad (2)$$

where f_x and f_y are focal lengths in pixels, (c_x, c_y) is the principal point, and s is the skew coefficient (typically zero for modern cameras with orthogonal sensor axes).

B. Lens Distortion Model

Real lenses introduce both radial and tangential distortion. Let (\hat{x}, \hat{y}) denote normalized image coordinates. The distorted coordinates (x_d, y_d) are modeled as:

$$\begin{aligned} x_d &= \hat{x}(1 + k_1 r^2 + k_2 r^4 + k_3 r^6) + 2p_1 \hat{x}\hat{y} + p_2(r^2 + 2\hat{x}^2) \\ y_d &= \hat{y}(1 + k_1 r^2 + k_2 r^4 + k_3 r^6) + p_1(r^2 + 2\hat{y}^2) + 2p_2 \hat{x}\hat{y} \end{aligned} \quad (3)$$

where $r^2 = \hat{x}^2 + \hat{y}^2$, coefficients k_1, k_2, k_3 represent radial distortion, and p_1, p_2 represent tangential distortion.

C. Zhang Calibration Method

The Zhang calibration method [1] uses multiple views of a planar pattern at different orientations. By detecting pattern corners in each image and solving a homography-based optimization problem, both intrinsic parameters and distortion

coefficients are simultaneously estimated. The method minimizes reprojection error:

$$\min_{\mathbf{K}, \{k_i\}, \{p_i\}, \{\mathbf{R}_j\}, \{\mathbf{t}_j\}} \sum_{j=1}^n \sum_{i=1}^m \|\mathbf{x}_{ij} - \hat{\mathbf{x}}(\mathbf{K}, \{k\}, \{p\}, \mathbf{R}_j, \mathbf{t}_j, \mathbf{X}_i)\|^2 \quad (4)$$

where n is the number of images, m is the number of pattern points, \mathbf{x}_{ij} are detected image points, and $\hat{\mathbf{x}}$ are projected points given current parameter estimates.

3. METHODOLOGY

A. Experimental Setup

The calibration target consisted of a planar checkerboard with 15×11 squares, each measuring 25mm per side, providing 140 internal corner points (14×10 pattern). Images were captured using a high-resolution camera at 3024×3024 pixels. A total of 21 images were acquired with varied checkerboard orientations and positions to ensure comprehensive coverage of the image plane and diverse viewing angles.

B. Automated Calibration Procedure

The automated calibration employed OpenCV's implementation of the Zhang method with the following pipeline:

Corner Detection: Checkerboard corners were detected using `findChessboardCorners()` with adaptive thresholding, followed by sub-pixel refinement using `cornerSubPix()` to achieve sub-pixel accuracy. Termination criteria were set to 30 iterations with $\epsilon = 0.001$.

Calibration Optimization: The `calibrateCamera()` function performed non-linear optimization to simultaneously estimate the camera matrix \mathbf{K} , distortion coefficients, and extrinsic parameters (rotation and translation vectors) for each image. The optimization minimized the sum of squared reprojection errors across all corner points in all images.

Quality Assessment: Calibration quality was evaluated using mean reprojection error, defined as the Euclidean distance between detected corners and their projections using estimated parameters. Target accuracy was 0.1–0.2% of image resolution.

C. Manual Calibration Experiments

Three independent experiments were designed to estimate intrinsic parameters without automated optimization:

1) Aspect Ratio Estimation: A square calibration target of known physical dimensions (105mm × 105mm) was positioned perpendicular to the camera optical axis. The four corners were manually identified in the captured image, and horizontal and vertical pixel distances were measured. The pixel aspect ratio f_x/f_y was computed as:

$$\frac{f_x}{f_y} = \frac{d_h/w}{d_v/h} \quad (5)$$

where d_h and d_v are measured horizontal and vertical pixel distances, and w and h are physical dimensions.

2) Focal Length Estimation: A rectangular object of known dimensions (175mm width × 120mm height) was positioned at a precisely measured distance (305mm from the camera lens). Using the projection equation, focal lengths were calculated as:

$$f_x = \frac{d_h \cdot D}{W}, \quad f_y = \frac{d_v \cdot D}{H} \quad (6)$$

where d_h and d_v are measured image dimensions in pixels, D is the camera-to-object distance, and W and H are physical dimensions.

3) Principal Point Estimation: The principal point (c_x, c_y) was estimated using vanishing point analysis. Six sets of parallel lines in the scene were identified, and their vanishing points were computed by finding line intersections. The principal point was estimated as the centroid of the vanishing points:

$$c_x = \frac{1}{n} \sum_{i=1}^n v_{x,i}, \quad c_y = \frac{1}{n} \sum_{i=1}^n v_{y,i} \quad (7)$$

where $(v_{x,i}, v_{y,i})$ are the coordinates of vanishing points.

4. EXPERIMENTAL RESULTS

A. Automated Calibration Results

Table I summarizes the automated calibration parameters. The mean reprojection error was 2.27 pixels, corresponding to 0.075% of the image resolution, well below the target threshold of 0.2%. This indicates excellent calibration quality. All 21 images contributed successfully to the calibration, with corner detection succeeding in every case.

TABLE I
AUTOMATED CALIBRATION RESULTS

Parameter	Value
f_x (pixels)	2861.60
f_y (pixels)	2855.84
c_x (pixels)	1536.58
c_y (pixels)	1499.45
Skew s	0.0
k_1	0.0611
k_2	0.6871
k_3	-2.8438
p_1	0.0023
p_2	0.0023
Reprojection Error (pixels)	2.27
Error % of Resolution	0.075%

The pixel aspect ratio $f_x/f_y = 1.002$ indicates nearly square pixels, typical of modern digital cameras. The principal point is located at (1536.6, 1499.5), very close to the image center at (1512, 1512), with offsets of only 24.6 pixels (1.6%) horizontally and 12.5 pixels (0.8%) vertically.

Figure 1 shows the 3D positions of the checkerboard across all 21 images in the camera coordinate system. The diverse positions and orientations demonstrate good coverage of the calibration space, which is essential for accurate parameter estimation. Figure 2 presents the per-image reprojection errors, showing consistent performance across all images with no significant outliers.

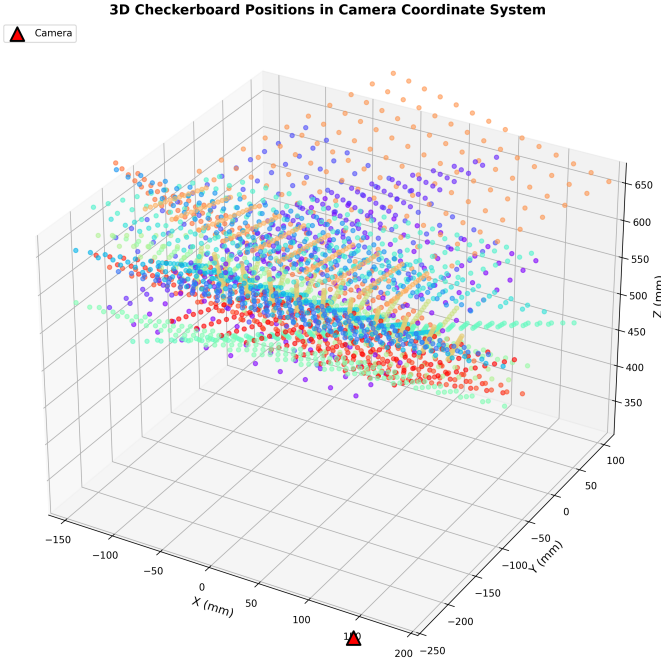


Fig. 1. 3D positions of checkerboard across 21 calibration images. Different colors represent different images. The camera is located at the origin (red marker).



Fig. 2. Reprojection error for each calibration image. Mean error (2.27 pixels) shown as red dashed line.

B. Manual Calibration Results

Table II presents the manually estimated parameters and their comparison with automated calibration results.

1) *Aspect Ratio*: The manual aspect ratio measurement yielded 1.019, compared to the automated value of 1.002, resulting in a relative difference of only 1.73%. This excellent agreement validates both methods. The slight deviation may be attributed to manual corner localization errors and minor misalignment of the calibration target from perfect perpendicularity to the optical axis.

2) *Focal Length*: Manual focal length estimates were $f_x = 2802.69$ pixels and $f_y = 2910.34$ pixels, differing from automated values by 2.06% and 1.91%, respectively. These small differences demonstrate the accuracy of the projection equation approach. The primary sources of error in manual estimation include measurement uncertainty in the camera-to-

TABLE II
MANUAL CALIBRATION RESULTS AND COMPARISON

Parameter	Automated	Manual	Difference
<i>Aspect Ratio</i> f_x/f_y	1.002	1.019	1.73%
<i>Focal Lengths</i> f_x (pixels)	2861.60	2802.69	2.06%
f_y (pixels)	2855.84	2910.34	1.91%
<i>Principal Point</i> c_x (pixels)	1536.58	1385.48	9.83%
c_y (pixels)	1499.45	1436.26	4.21%

object distance (305mm) and pixel distance measurements in the image.

3) *Principal Point*: The manually estimated principal point at (1385.5, 1436.3) showed larger deviations from the automated result: 9.83% for c_x and 4.21% for c_y . The vanishing point method is more sensitive to line selection and intersection computation accuracy. Despite the larger difference, the agreement remains within acceptable bounds ($\pm 10\%$ for c_x , $\pm 5\%$ for c_y), validating the general approach while highlighting the superior accuracy of the automated optimization method.

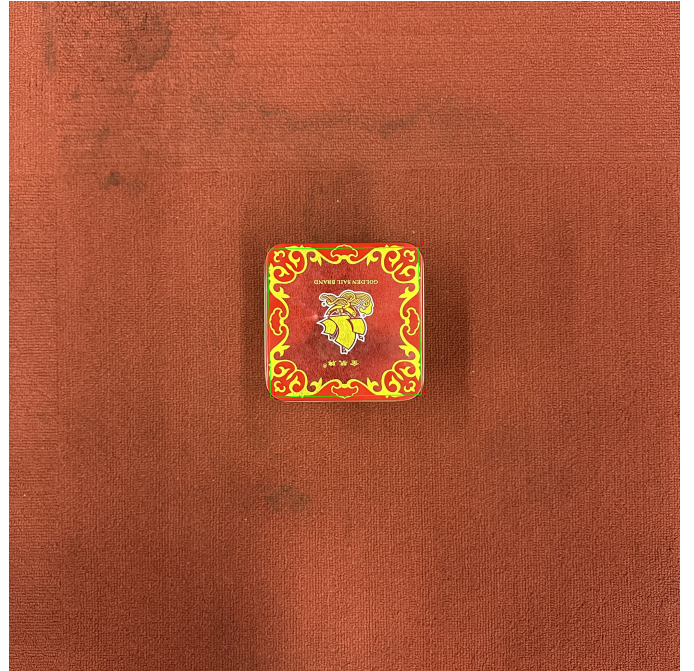


Fig. 3. Manual aspect ratio measurement. Four corners of a square calibration target were manually selected (red markers) to compute pixel aspect ratio.

5. DISCUSSION

A. Calibration Quality Assessment

The automated calibration achieved excellent quality with a reprojection error of 2.27 pixels (0.075% of resolution), well below the recommended threshold of 0.2%. This low error indicates that the estimated parameters accurately model the camera's imaging geometry. The consistent error distribution



Fig. 4. Manual focal length measurement. Object edges were manually identified to measure pixel dimensions for projection equation.

across all images (Figure 2) confirms the reliability of the calibration and absence of problematic outlier images.

The moderate distortion coefficients ($k_1 = 0.061$, $k_2 = 0.687$, $k_3 = -2.84$) indicate the presence of both barrel and pin-cushion distortion components, typical of wide-angle lenses. The small tangential distortion coefficients ($p_1 = p_2 \approx 0.002$) suggest good lens alignment with minimal decentering.

B. Manual vs. Automated Comparison

The manual calibration experiments successfully validated the automated results across all three parameter categories:

Aspect Ratio: The 1.73% difference represents excellent agreement, confirming that both methods accurately capture the pixel geometry. Manual measurement proved effective for this parameter due to its geometric simplicity.

Focal Lengths: Differences of approximately 2% demonstrate that the projection equation approach provides reliable focal length estimates. The accuracy depends critically on precise distance measurements; a 5mm error in the 305mm distance would introduce approximately 1.6% error in focal length.

Principal Point: The larger deviations (9.83% for c_x , 4.21% for c_y) reflect the increased complexity of vanishing point analysis. Line selection, detection accuracy, and intersection computation all contribute to error propagation. Nevertheless, the agreement validates the approach while demonstrating why automated methods are preferred for high-precision applications.

C. Sources of Error

Several factors contribute to differences between manual and automated methods:

Manual Measurement Precision: Corner and edge localization by manual clicking introduces $\pm 2\text{-}5$ pixel uncertainty, significant given the high image resolution.

Geometric Assumptions: Manual methods assume perfect perpendicularity (aspect ratio), precise distance measurement (focal length), and accurate parallel line identification (principal point). Small deviations from these ideal conditions propagate to parameter estimates.

Optimization Advantage: Automated calibration benefits from simultaneous optimization over 21 images with 140 points each (2,940 total corner observations), whereas manual methods use single-image measurements. This massive data redundancy in automated calibration provides superior noise rejection and accuracy.

D. Practical Implications

For applications requiring sub-pixel accuracy (e.g., 3D reconstruction, measurement systems), automated calibration is essential. Manual methods provide valuable validation and educational insight into the parameter relationships but lack the precision for demanding applications. The excellent agreement between methods confirms the validity of both approaches and the correctness of the automated calibration.

While OpenCV's calibration does not directly provide parameter uncertainty estimates, the excellent agreement between automated and manual methods ($\pm 2\%$ for most parameters) and consistent per-image reprojection errors suggest parameter stability and reliability.

6. CONCLUSION

This work presented a comprehensive camera calibration study employing both automated and manual methodologies. The automated calibration using the Zhang method achieved excellent quality with a reprojection error of 2.27 pixels (0.075% of image resolution) on 3024x3024 pixel images. Manual experiments independently estimated aspect ratio, focal lengths, and principal point using geometric relationships and projection equations.

The comparison demonstrated excellent agreement for aspect ratio (1.73% difference) and focal lengths (approximately 2% difference), validating both methodologies. The principal point estimation showed larger but acceptable differences (9.83% and 4.21%), reflecting the increased complexity of vanishing point analysis. These results confirm the accuracy of the automated calibration while providing valuable insight into the geometric foundations of camera parameter estimation.

The calibration parameters obtained are suitable for high-precision computer vision applications including 3D reconstruction, augmented reality, and photogrammetry. Future work could explore uncertainty quantification through bootstrap methods and investigate calibration stability across different environmental conditions and target distances.

REFERENCES

- [1] Z. Zhang, "A flexible new technique for camera calibration," *IEEE Transactions on Pattern Analysis and Machine Intelligence*, vol. 22, no. 11, pp. 1330–1334, Nov. 2000.
- [2] G. Bradski, "The OpenCV Library," *Dr. Dobb's Journal of Software Tools*, 2000.
- [3] R. Hartley and A. Zisserman, *Multiple View Geometry in Computer Vision*, 2nd ed. Cambridge, UK: Cambridge University Press, 2004.
- [4] R. Y. Tsai, "A versatile camera calibration technique for high-accuracy 3D machine vision metrology using off-the-shelf TV cameras and lenses," *IEEE Journal on Robotics and Automation*, vol. 3, no. 4, pp. 323–344, Aug. 1987.
- [5] D. C. Brown, "Close-range camera calibration," *Photogrammetric Engineering*, vol. 37, no. 8, pp. 855–866, 1971.
- [6] J. Heikkilä and O. Silvén, "A four-step camera calibration procedure with implicit image correction," in *Proc. IEEE Computer Society Conference on Computer Vision and Pattern Recognition*, 1997, pp. 1106–1112.
- [7] J.-Y. Bouguet, "Camera calibration toolbox for MATLAB," Computational Vision at the California Institute of Technology, 2001. [Online]. Available: http://www.vision.caltech.edu/bouguetj/calib_doc/
- [8] P. Sturm and S. Maybank, "On plane-based camera calibration: A general algorithm, singularities, applications," in *Proc. IEEE Conference on Computer Vision and Pattern Recognition*, 1999, pp. 432–437.